Article:
Ruderman, M.S. (2017) Compressibility Effect on the Rayleigh–Taylor Instability with Sheared Magnetic Fields. Solar Physics, 292. 47. ISSN 0038-0938

https://doi.org/10.1007/s11207-017-1073-8

Solar Physics
DOI: 10.1007/•••••-•••-•••-••••-•

Compressibility Effect on the Rayleigh-Taylor Instability with Sheared Magnetic Fields

M.S. Ruderman[1,2]

00, 0000

Abstract We study the effect of plasma compressibility on the Rayleigh-Taylor instability of a magnetic interface with sheared magnetic field. We assume that the plasma is ideal and the equilibrium quantities are constant above and below the interface. We derive the dispersion equation. Written in dimensionless variables it contains seven dimensionless parameters: The ratio of plasma densities above and below the interface ζ, the ratio of magnetic field magnitude squared χ, the shear angle α, the plasma beta above and below the interface, β_2 and β_1, the angle between the perturbation wavenumber and the magnetic field direction above the interface ϕ, and the dimensionless wavenumber κ. Only six of them are independent because χ, β_1, and β_2 are related by the condition of total pressure continuity at the interface. Only perturbations with the wavenumber smaller than the critical wavenumber are unstable. The critical wavenumber depends on ϕ, but it is independent of β_1 and β_2, and is the same as that in the incompressible plasma approximation. The dispersion equation is solved numerically with $\zeta = 100$, $\chi = 1$, and $\beta_1 = \beta_2 = \beta$. We obtain the following results. When β decreases, so does the maximum instability increment. However the effect is very moderate. It is more pronounced for large values of α. We also calculate the dependence on ϕ of the maximum instability increment with respect to κ. The instability increment takes its maximum at $\phi = \phi_{\rm m}$. Again the decrease of β results in the reduction of the instability increment. This reduction is more pronounced for large values of $|\phi - \phi_{\rm m}|$. When both α and $|\phi - \phi_{\rm m}|$ are small the reduction effect is practically negligible. The theoretical results are applied to the magnetic Rayleigh-Taylor instability of prominence threads in the solar atmosphere.

Keywords: Sun, Corona · Magnetic Fields · Magnetohydrodynamics · stability

[1]Solar Physics and Space Plasma Research Centre (SP^{2}RC),
School of Mathematics and Statistics, University of Sheffield,
Hicks Building, Hounsfield Road, Sheffield, S3 7RH, UK
e-mail: m.s.ruderman@sheffield.ac.uk
[2]Space Research Institute (IKI), Russian Academy of
Sciences, Moscow, Russia

1. Introduction

The magnetic Rayleigh-Taylor (MRT) instability operates in a variety of astrophysical systems. For example, it manifests itself in buoyant magnetised bubbles observed in clusters of galaxies (Robinson *et al.*, 2004; Jones and De Young, 2005; Owen, De Young, and Jones, 2009), in shells of young supernova remnants (Jun, Norman, and Stone, 1995; Jun and Norman, 1996), and at the interface between an expanding pulsar wind nebula and its surrounding supernova remnant (Bucciantini *et al.*, 2004).

The MRT instability also plays an important role in solar physics. Isobe *et al.* (2005, 2006) suggested that the MRT instability possibly causes the filamentation of mass and current density in emerging flux regions. Ryutova *et al.* (2010) proposed that several dynamic processes operating in prominences are most probably caused by MRT instabilities. Hillier *et al.* (2011, 2012a, b) have carried out three-dimensional magnetohydrodynamic simulations to study the nonlinear evolution of the Kippenhahn-Shlüter prominence model caused by the MRT instability.

The MRT instability also might affect magnetic threads in solar prominences. The threads are parts of a magnetic tube filled with the cold plasma with a large density contrast with respect to the coronal plasma. They are very thin, of the order of 100 km, aligned with the magnetic field and often they seem to be horizontal with respect to the photosphere. The threads have relatively low temperature meaning that the thread plasma is only partially ionized. The MRT instability in partially ionized plasmas has been studied both analytically (Díaz, Khomenko, and Collados, 2014) and numerically (Khomenko *et al.*, 2014).

Observations show that the threads have short lifetimes, typically of the order of 10 min only. This observation inspired Terradas, Oliver, and Ballester (2012) to propose that the magnetic Rayleigh-Taylor instability could be responsible for this phenomenon. They considered a very simple model. The thread was assumed to be a Cartesian slab permeated by a horizontal magnetic field that has the same direction inside the thread and in the surrounding hot plasma. A drawback of this model is that the instability growth rate is unbounded. Perturbations with an arbitrary wavelength propagating in the direction orthogonal to the magnetic field are unstable and the perturbation increment tends to infinity when the wavelength tends to zero.

Ruderman, Terradas, and Ballester (2014) improved the model suggested by Terradas, Oliver, and Ballester (2012) by including magnetic shear. They studied the MRT instability of both a single magnetic interface and a slab. In particular, they found that the maximum increment is inversely proportional to the angle between the magnetic field direction inside the thread and in the external plasma. Assuming that the thread lifetime is equal to the inverse of the maximum increment they managed to estimate the shear angle. Ruderman (2015) studied the effect of flow in a thread on the estimation of the shear angle and found that this effect is minor.

Terradas, Oliver, and Ballester (2012), Ruderman, Terradas, and Ballester (2014), and Ruderman (2015) used the approximation of incompressible plasma

to study the MRT instability. The effect of compressibility on the Rayleigh-Taylor instability was studied by a number of authors. For example, Baker (1983) and Livescu (2004) studied the effect of compressibility on the RT instability in unmagnetised fluids. In particular, they showed that the instability increment decreases when the ratio of fluid densities at the interface and the ratio of specific heats γ are fixed, while the sound speed decreases. The compressibility effect on the MRT instability was also studied. Liberatore and Bouquet (2008) analytically studied this problem in the linear approximation for the equilibrium where the magnetic field has the same direction at the two sides of the interface. Only perturbations with the wavevector either parallel or perpendicular to the equilibrium magnetic field were considered. Liberatore *et al.* (2009) studied the same problem numerically and compared the numerical and analytical results. Stone and Gardiner (2007a) and Stone and Gardiner (2007b) studied the nonlinear MRT instability numerically for various forms of the equilibrium magnetic field.

This article aims to investigate the compressibility effect on the MRT instability in the presence of magnetic shear. The paper is organised as follows. In the next section we formulate the problem and write down the main equations and boundary conditions. In Section 3 we derive the dispersion equation determining the increment of unstable normal modes. In Section 4 we investigate the dispersion equation both analytically and numerically. In Section 5 we apply the obtained results to the stability of prominence threads. Section 6 contains the summary of the obtained results and our conclusions.

2. Problem Formulation

We consider the stability of a tangential discontinuity that, in the absence of flow, is also called a magnetic interface, in an inviscid infinitely conducting plasma. We also neglect thermal conduction, so that the plasma motion is described by the ideal magnetohydrodynamic (MHD) equations. The equilibrium configuration is shown in Figure 1. The equilibrium magnetic field, density and pressure are $\boldsymbol{B}$, ρ, and p. There is no equilibrium flow. The superscripts 1 and 2 refer to the quantities below and above the interface, respectively. The z-axis of Cartesian coordinates is antiparallel to the gravity acceleration $\boldsymbol{g}$, meaning that $\boldsymbol{g} = -g\boldsymbol{e}_z$, where $\boldsymbol{e}_z$ is the unit vector in the z-direction. The equation of the unperturbed interface is $z = 0$. The equilibrium magnetic field is in the x-direction above the interface. The angle between the equilibrium magnetic field direction below and above the interface is α. The equilibrium quantities only depend on z and they are related by the equation

$$\frac{\mathrm{d}}{\mathrm{d}z}\left(p + \frac{B^2}{2\mu_0}\right) = -g\rho, \tag{1}$$

where μ_0 is the magnetic permeability of free space. They also satisfy the condition of the total pressure balance at the interface,

$$p_1 + \frac{B_1^2}{2\mu_0} = p_2 + \frac{B_2^2}{2\mu_0}. \tag{2}$$

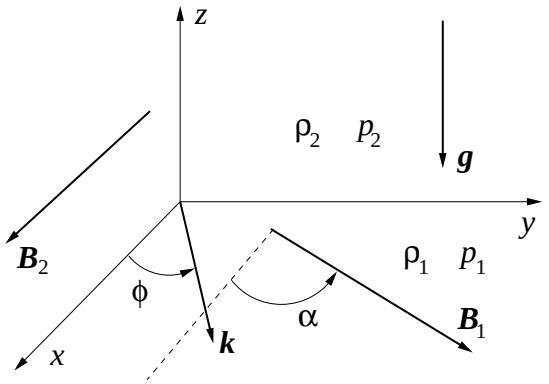

Figure 1. Sketch of the equilibrium.

The perturbed plasma motion is described by the linearised equations of ideal MHD:

$$\frac{\partial \rho'}{\partial t} + \nabla \cdot (\rho \boldsymbol{v}) = 0, \tag{3}$$

$$\rho \frac{\partial \boldsymbol{v}}{\partial t} = -\nabla P + \frac{1}{\mu_0}(\boldsymbol{B} \cdot \nabla)\boldsymbol{b} + \frac{b_z}{\mu_0}\frac{\mathrm{d}\boldsymbol{B}}{\mathrm{d}z} - g\rho'\boldsymbol{e}_z, \tag{4}$$

$$\frac{\partial \boldsymbol{b}}{\partial t} = (\boldsymbol{B} \cdot \nabla)\boldsymbol{v} - \boldsymbol{B}\nabla \cdot \boldsymbol{v} - v_z\frac{\mathrm{d}\boldsymbol{B}}{\mathrm{d}z}, \tag{5}$$

$$\frac{\partial}{\partial t}\left(\frac{p' - c_\mathrm{s}^2\rho'}{\rho^\gamma}\right) + \boldsymbol{v} \cdot \nabla\left(\frac{p}{\rho^\gamma}\right) = 0, \tag{6}$$

where $\boldsymbol{v} = (v_x, v_y, v_z)$ is the plasma velocity, $\boldsymbol{b} = (b_x, b_y, b_z)$ the magnetic field perturbation, ρ' is the density perturbation, p' the pressure perturbation, P the perturbation of the total pressure given by

$$P = p' + \frac{\boldsymbol{b} \cdot \boldsymbol{B}}{\mu_0}, \tag{7}$$

and c_s is the sound speed defined by $c_\mathrm{s}^2 = \gamma p/\rho$. Below we assume that the temperature is constant both in region 1 and region 2 meaning that c_s is constant in both regions. Equation (6) is the equation of entropy conservation.

Equations (3)–(6) must be supplemented with the boundary conditions at $z = 0$. We introduce the following notation for the jump of function $f(z)$ across the interface:

$$[\![f]\!] = \lim_{z \to +0}[f(z) - f(-z)].$$

The first boundary condition is the kinematic boundary condition that expresses the continuity of the normal component of plasma displacement at the interface. In the absence of equilibrium flow it reduces in the linear approximation to a

very simple form,

$$[\![v_z]\!] = 0. \tag{8}$$

The second boundary condition is the dynamic boundary condition expressing the continuity of the total pressure. It is written as

$$\left[\!\!\left[p + p' + \frac{|\boldsymbol{B}+\boldsymbol{b}|^2}{2\mu_0} \right]\!\!\right] = 0 \quad \text{at} \quad z = h(t,x,y),$$

where $z = h(t,x,y)$ is the equation of the perturbed surface of the interface. Linearising this equation and using Equation (1) yields

$$[\![P - g\rho h]\!] = 0 \quad \text{at} \quad z = 0.$$

Differentiating this equation with respect to time and using the equation $v_z = \partial h/\partial t$ valid in the linear approximation at $z = 0$ to eliminate h, we eventually arrive at

$$\left[\!\!\left[g\rho v_z - \frac{\partial P}{\partial t} \right]\!\!\right] = 0. \tag{9}$$

Consider as an example the MRT instability of the interface between a partially ionized cold plasma in a prominence and a hot surrounding plasma. We will see below that a perturbation in the form of a harmonic wave with the wavenumber k decays at a distance of the order of $1/k$ from the interface, which is approximately one sixth of the wavelength. We will only consider perturbations with the wavelength not exceeding the characteristic scale of the equilibrium quantity variation. This enables us to neglect the variation of the equilibrium quantities with the height and take them as constant.

We will see in Section 5 that the fastest growing perturbations have wavelengths of a few Mm. Even if we assume that $B_1 = \text{const}$, we obtain that the characteristic scale of the equilibrium density and pressure variation in region 1 is about 50 Mm. Hence, the condition that the perturbation wavelengths do not exceed the characteristic length of the equilibrium quantity variation in region 1 is definitely satisfied.

However the situation with region 2 is not so obvious. If we assume that $B_2 = \text{const}$, then we obtain that the characteristic scale of the equilibrium density and pressure variation in region 2 is about 0.5 Mm, and it can be even smaller if we take into account that the prominence plasma is only partially ionized. However the plasma beta is usually small both in the hot coronal and cold prominence plasma. Then, in accordance with Equation (1), the magnetic pressure variation with height can substantially increase the characteristic scale of equilibrium quantity variation. We assume that both the plasma and magnetic pressure are proportional to $\exp(-z/H_2)$. Then it follows from Equations (1) that in region $z > 0$

$$\rho = \rho_2 \mathrm{e}^{-z/H_2},\ p = p_2 \mathrm{e}^{-z/H_2},\ B = B_2 \mathrm{e}^{-z/2H_2},\ H_1 = \frac{p_2(1+\bar{\beta})}{g\rho_2\bar{\beta}},\ \bar{\beta} = \frac{2\mu_0 p_2}{B_2^2}, \tag{10}$$

where ρ_2, p_2, B_2 are the values of the equilibrium density, pressure, and magnetic field magnitude at the interface. However this equilibrium is convectively unstable when $\bar{\beta} < 1/(\gamma - 1)$ (Yu, 1965). Its increment is given by (Newcomb, 1961)

$$\Gamma = \frac{g}{c_{\mathrm{A}2}} \left(1 - \sqrt{\frac{\gamma \bar{\beta}}{1 + \bar{\beta}}} \right), \tag{11}$$

where c_{A} is the Alfvén speed defined by

$$c_{\mathrm{A}}^2 = \frac{B^2}{\mu_0 \rho}. \tag{12}$$

In particular, $\Gamma \approx g/c_{\mathrm{A}2}$ when $\bar{\beta} \ll 1$. The convective instability can affect the MRT instability. When we neglect the variation of equilibrium quantities in region 2, we neglect the possible effect of convective instability on the MRT instability. It seems that the effect of convective instability can be neglected if its increment is much smaller than the increment of the MRT instability. We make this *apriori* assumption, which enables us to neglect the equilibrium quantity variation in region 2. We will verify that this assumption is satisfied when applying the results obtained in this article to the MRT instability in solar prominences.

Equations (3)–(6) with the constant equilibrium quantities reduce to

$$\frac{\partial \rho'}{\partial t} + \rho \nabla \cdot \boldsymbol{v} = 0, \tag{13}$$

$$\rho \frac{\partial \boldsymbol{v}}{\partial t} = -\nabla P + \frac{1}{\mu_0} (\boldsymbol{B} \cdot \nabla) \boldsymbol{b} - g \rho' \boldsymbol{e}_z, \tag{14}$$

$$\frac{\partial \boldsymbol{b}}{\partial t} = (\boldsymbol{B} \cdot \nabla) \boldsymbol{v} - \boldsymbol{B} \nabla \cdot \boldsymbol{v}, \tag{15}$$

$$p' = c_{\mathrm{s}}^2 \rho'. \tag{16}$$

These equations with the boundary conditions Equations (8) and (9) are used in the next section to derive the dispersion equation for normal modes.

3. Derivation of the Dispersion Equation

We Fourier-analyse the perturbations of all quantities and take them proportional to $\exp[i(\boldsymbol{k} \cdot \boldsymbol{r} - \omega t)]$, where $\boldsymbol{k} = (k_x, k_y, 0)$ and $\boldsymbol{r} = (x, y, z)$. We write $\boldsymbol{v}$ and $\boldsymbol{b}$ as

$$\boldsymbol{v} = \boldsymbol{v}_\perp + v_z \boldsymbol{e}_z, \quad \boldsymbol{b} = \boldsymbol{b}_\perp + b_z \boldsymbol{e}_z. \tag{17}$$

As a result we reduce the system of Equations (13)–(16) to

$$i\omega \rho' - \rho \left(\frac{\mathrm{d} v_z}{\mathrm{d} z} + i \boldsymbol{k} \cdot \boldsymbol{v}_\perp \right) = 0, \tag{18}$$

$$\rho\omega\boldsymbol{v}_\perp = \boldsymbol{k}P - \frac{(\boldsymbol{k}\cdot\boldsymbol{B})\boldsymbol{b}_\perp}{\mu_0}, \tag{19}$$

$$i\rho\omega v_z = \frac{\mathrm{d}P}{\mathrm{d}z} - \frac{i(\boldsymbol{k}\cdot\boldsymbol{B})b_z}{\mu_0} + g\rho', \tag{20}$$

$$i\omega\boldsymbol{b}_\perp = -i(\boldsymbol{k}\cdot\boldsymbol{B})\boldsymbol{v}_\perp + \boldsymbol{B}\left(\frac{\mathrm{d}v_z}{\mathrm{d}z} + i\boldsymbol{k}\cdot\boldsymbol{v}_\perp\right), \tag{21}$$

$$\omega b_z = -(\boldsymbol{k}\cdot\boldsymbol{B})v_z, \tag{22}$$

$$p' = c_\mathrm{s}^2\rho'. \tag{23}$$

The boundary condition Equation (8) does not change, while the boundary condition Equation (9) is transformed to

$$[\![g\rho v_z + i\omega P]\!] = 0 \quad \text{at} \;\; z = 0. \tag{24}$$

We now introduce the angle φ between $\boldsymbol{k}$ and $\boldsymbol{B}$ meaning that $\boldsymbol{k}\cdot\boldsymbol{B} = kB\cos\varphi$. We have $\varphi_1 = \phi - \alpha$ and $\varphi_2 = \phi$ (see Figure 1). It is shown in Appendix A that the system of Equations (18)–(23) can be reduced to the system of two equations for v_z and P:

$$P = -\frac{i\rho\Omega_\mathrm{A}\Omega_\mathrm{T}\left(c_\mathrm{s}^2 + c_\mathrm{A}^2\right)}{\omega D}\frac{\mathrm{d}v_z}{\mathrm{d}z}, \tag{25}$$

$$\frac{\mathrm{d}P}{\mathrm{d}z} + \frac{gk^2}{\omega^2}P = \frac{i\rho\Omega_\mathrm{A}}{\omega}\left(\frac{g}{\omega^2}\frac{\mathrm{d}v_z}{\mathrm{d}z} + v_z\right), \tag{26}$$

where

$$D = \omega^4 - \omega^2k^2\left(c_\mathrm{s}^2 + c_\mathrm{A}^2\right) + k^4c_\mathrm{s}^2c_\mathrm{A}^2\cos^2\varphi, \tag{27}$$

$$\Omega_\mathrm{A} = \omega^2 - k^2c_\mathrm{A}^2\cos^2\varphi, \tag{28}$$

$$\Omega_\mathrm{T} = \omega^2 - k^2c_\mathrm{T}^2\cos^2\varphi, \quad c_\mathrm{T}^2 = \frac{c_\mathrm{s}^2c_\mathrm{A}^2}{c_\mathrm{s}^2 + c_\mathrm{A}^2}. \tag{29}$$

Substituting Equation (25) in Equation (26) yields

$$\Omega_\mathrm{T}\left(c_\mathrm{s}^2 + c_\mathrm{A}^2\right)\frac{\mathrm{d}^2v_z}{\mathrm{d}z^2} + g\omega^2\frac{\mathrm{d}v_z}{\mathrm{d}z} + Dv_z = 0. \tag{30}$$

Below we only consider unstable wave modes. Since in static MHD the square of an eigenfrequency is real (*e.g.* Goedbloed and Poedts, 2004), this implies that we only consider $\omega^2 < 0$. Then it follows that $\Omega_\mathrm{T} < 0$ and $D > 0$. Consequently the characteristic equation of Equation (30) has two real roots, one positive and the other negative. The perturbations must decay as $|z| \to \infty$. Hence we must choose the solution corresponding to the positive root of the characteristic equation in region 1, and the solution corresponding to the negative root of the

characteristic equation in region 2. As a result we obtain that the solution to Equation (30) satisfying the boundary condition Equation (8) is given by

$$v_z = \exp\left(-\frac{g\omega^2 z}{2\Omega_{\rm T}\left(c_{\rm s}^2+c_{\rm A}^2\right)}\right)\begin{cases} {\rm e}^{\lambda_1 z}, & z<0,\\ {\rm e}^{-\lambda_2 z}, & z>0,\end{cases} \tag{31}$$

where

$$\lambda = -\frac{\sqrt{g^2\omega^4 - 4D\Omega_{\rm T}\left(c_{\rm s}^2+c_{\rm A}^2\right)}}{2\Omega_{\rm T}\left(c_{\rm s}^2+c_{\rm A}^2\right)}. \tag{32}$$

When deriving Equation (31) we have taken into account that the solution to a linear problem is defined with the accuracy of an arbitrary multiplicative constant. Substituting Equation (31) in Equation (25) yields

$$P = \frac{i\rho\Omega_{\rm A}}{2\omega D}\exp\left(\frac{-g\omega^2 z}{2\Omega_{\rm T}\left(c_{\rm s}^2+c_{\rm A}^2\right)}\right)\begin{cases} \left[g\omega^2 - 2\lambda_1\Omega_{\rm T1}\left(c_{\rm s1}^2+c_{\rm A1}^2\right)\right]{\rm e}^{\lambda_1 z}, & z<0,\\ \left[g\omega^2 + 2\lambda_2\Omega_{\rm T2}\left(c_{\rm s2}^2+c_{\rm A2}^2\right)\right]{\rm e}^{-\lambda_2 z}, & z>0.\end{cases} \tag{33}$$

Substituting Equations (31) and (33) in the boundary conditions Equation (24) we obtain the dispersion equation

$$\begin{aligned} &g\rho_1 - \frac{\rho_1\Omega_{\rm A1}}{2D_1}\left[g\omega^2 - 2\lambda_1\Omega_{\rm T1}\left(c_{\rm s1}^2+c_{\rm A1}^2\right)\right]\\ &= g\rho_2 - \frac{\rho_2\Omega_{\rm A2}}{2D_2}\left[g\omega^2 + 2\lambda_2\Omega_{\rm T2}\left(c_{\rm s2}^2+c_{\rm A2}^2\right)\right]. \end{aligned} \tag{34}$$

This dispersion relation is used in the next section to study the Rayleigh-Taylor instability.

4. Investigation of Dispersion Equation

We introduce the dimensionless quantities

$$\zeta = \frac{\rho_2}{\rho_1}, \quad \kappa = \frac{kc_{\rm A2}^2}{g}, \quad \sigma = -\frac{i\omega c_{\rm A2}}{g}, \quad \chi = \frac{B_1^2}{B_2^2}, \quad \beta_{1,2} = \frac{c_{\rm s1,2}^2}{c_{\rm A1,2}^2}, \tag{35}$$

to rewrite Equation (34) in the dimensionless form

$$\frac{\zeta\Psi_2}{\Delta_2}\left(\sigma^2 + \sqrt{\sigma^4 + 4\Delta_2\Phi_2}\right) - \frac{\Psi_1}{\Delta_1}\left(\sigma^2 - \sqrt{\sigma^4 + 4\chi\zeta\Delta_1\Phi_1}\right) = 2\zeta - 2, \tag{36}$$

where

$$\Psi_1 = \sigma^2 + \chi\zeta\kappa^2\cos^2(\phi-\alpha), \tag{37}$$

$$\Psi_2 = \sigma^2 + \kappa^2\cos^2\phi, \tag{38}$$

$$\Phi_1 = \sigma^2(\beta_1+1) + \beta_1\chi\zeta\kappa^2\cos^2(\phi-\alpha), \tag{39}$$

$$\Phi_2 = \sigma^2(\beta_2 + 1) + \beta_2\kappa^2\cos^2\phi, \tag{40}$$

$$\Delta_1 = \sigma^4 + \chi\zeta\kappa^2\sigma^2(\beta_1 + 1) + \beta_1\chi^2\zeta^2\kappa^4\cos^2(\phi - \alpha), \tag{41}$$

$$\Delta_2 = \sigma^4 + \kappa^2\sigma^2(\beta_2 + 1) + \beta_2\kappa^4\cos^2\phi. \tag{42}$$

Note that in plasma physics the standard definition of beta is that it is the ratio of the plasma to magnetic pressure. However here it is more convenient to define it as the ratio of the sound to Alfvén speed squared. The dimensionless parameters defined by Equation (35) are not independent. It follows from Equation (2) that there is the relation

$$\chi(2\beta_1 + \gamma) = 2\beta_2 + \gamma. \tag{43}$$

Since we only consider unstable modes it follows that $\sigma > 0$.

4.1. Analytical Results

We start by considering the case of an incompressible plasma. To obtain the dispersion relation in this case we take $c_\mathrm{s} \to \infty$. Then it is straightforward to show that Equation (36) reduces to

$$\sigma^2 = \frac{\kappa(\zeta - 1) - \zeta\kappa^2\left[\chi\cos^2(\phi - \alpha) + \cos^2\phi\right]}{\zeta + 1}. \tag{44}$$

This equation coincides with the dispersion equation obtained by Ruderman, Terradas, and Ballester (2014) (see Equation (19) in their paper). Below we briefly describe the results obtained by these authors. When the angle ϕ is fixed the corresponding eigenmode is unstable for

$$\kappa < \kappa_\mathrm{c}(\phi) = \frac{\zeta - 1}{\zeta\left[\chi\cos^2(\phi - \alpha) + \cos^2\phi\right]}. \tag{45}$$

Note that κ_c is independent of ϕ when $\chi = 1$ and $\alpha = \pi/2$. The dependence of κ_c on ϕ is shown in Figure 2 for various values of α. All perturbations with the dimensionless wavenumber satisfying

$$\kappa \geq \overline{\kappa}_\mathrm{c} = \max_\phi \kappa_\mathrm{c}(\phi) = \frac{\zeta - 1}{2\chi\zeta\sin^2\alpha}\left(\chi + 1 + \sqrt{\chi^2 + 2\chi\cos 2\alpha + 1}\right) \tag{46}$$

are stable. On the other hand, all perturbations with the dimensionless wavenumber satisfying

$$\kappa \leq \hat{\kappa}_\mathrm{c} = \min_\phi \kappa_\mathrm{c}(\phi) = \frac{\zeta - 1}{2\chi\zeta\sin^2\alpha}\left(\chi + 1 - \sqrt{\chi^2 + 2\chi\cos 2\alpha + 1}\right) \tag{47}$$

are unstable for any value of ϕ.

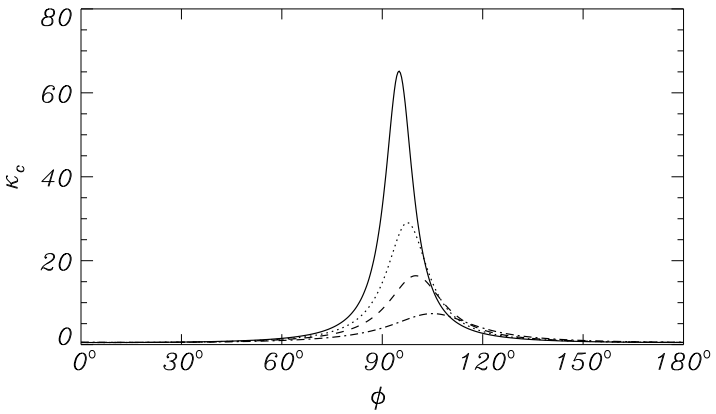

Figure 2. The dependence of κ_c on ϕ. The solid, dotted, dashed, and dashed-dotted curves correspond to $\alpha = 10°$, $15°$, $20°$, and $30°$, respectively.

When the angle ϕ is fixed the eigenmode with $\kappa = \kappa_m(\phi) = \frac{1}{2}\kappa_c(\phi)$ has the maximum increment. It is given by

$$\max_{\kappa} \sigma = \frac{\zeta - 1}{2\sqrt{\zeta(\zeta+1)\left[\chi \cos^2(\phi - \alpha) + \cos^2\phi\right]}}. \tag{48}$$

The maximum instability increment is

$$\sigma_m = \max_{\kappa,\phi} \sigma = \frac{\zeta - 1}{2\sin\alpha}\sqrt{\frac{\chi + 1 + \sqrt{\chi^2 + 2\chi\cos 2\alpha + 1}}{2\chi\zeta(\zeta+1)}}. \tag{49}$$

This maximum is obtained when $\kappa = \overline{\kappa}_m = \frac{1}{2}\overline{\kappa}_c$ and

$$\phi = \phi_m = \frac{1}{2}\arctan\frac{\chi \sin 2\alpha}{1 + \chi\cos 2\alpha} + \frac{\pi}{2}. \tag{50}$$

Since, as we have already noted, ω^2 must be real, the transition from stable to unstable modes occurs when ω^2 changes sign from positive to negative. This implies that the critical wavenumber corresponding to this transition is determined by Equation (34) with $\sigma = 0$. Then it is straightforward to show that the dimensionless critical wavenumber is given by Equation (45). Hence, we see that the compressibility does not affect the critical wavenumber. This implies that if a wavemode is stable/unstable in the limit of incompressible plasma, then it is stable/unstable when the compressibility is taken into account.

Now we obtain the approximate expressions for $\overline{\kappa}_m$ and σ_m valid for $\alpha \ll 1$. It follows from Equations (46), (49), and (50) that, in the approximation of incompressible plasmas, $\overline{\kappa}_m = \mathcal{O}(\alpha^{-2})$, $\overline{\kappa}_m = \mathcal{O}(\alpha^{-1})$, and $\pi/2 - \phi_m = \mathcal{O}(\alpha)$. We assume these scalings remain the same for any values of β_1 and β_2. This

inspires us to introduce the scaled quantities

$$\widetilde{\kappa} = \alpha^2 \kappa, \quad \widetilde{\sigma} = \alpha\sigma, \quad \widetilde{\phi} = \alpha^{-1}\left(\phi - \frac{\pi}{2}\right). \tag{51}$$

Substituting these expressions in Equation (36) and collecting terms of the leading order with respect to α we obtain

$$\widetilde{\sigma}^2 \approx \frac{\widetilde{\kappa}(\zeta - 1) - \zeta\widetilde{\kappa}^2[\chi(\widetilde{\phi} - 1)^2 + \widetilde{\phi}^2]}{\zeta - 1}. \tag{52}$$

Now, using this result and returning to the non-scaled variables yields

$$\overline{\kappa}_{\mathrm{m}} \approx \frac{(\zeta - 1)(\chi + 1)}{2\chi\zeta\alpha^2}, \quad \sigma_{\mathrm{m}} \approx \frac{\zeta - 1}{2\alpha}\sqrt{\frac{\chi + 1}{\chi\zeta(\zeta + 1)}}. \tag{53}$$

We see that the approximate expressions for $\overline{\kappa}_{\mathrm{m}}$ and σ_{m} are independent of β_1 and β_2, and the expressions for them can be obtained from the corresponding expressions in the incompressible plasma approximation when $\alpha \ll 1$.

4.2. Numerical Results

We see that σ depends on seven dimensionless parameters: ζ, χ, β_1, β_2, κ, ϕ, and α, of which only six are independent (recall that χ, β_1, and β_2 are related by Equation (44)). The left-hand side of Equation (36) is a periodic function of both ϕ and α, and the period with respect to each of these two angles is π. In addition, it is invariant under the substitution $\pi - \varphi \to \varphi$ and $\pi - \alpha \to \alpha$. This observation enables us to restrict the intervals of variation of these two angles to $0 \le \phi < \pi$ and $0 \le \alpha \le \pi/2$.

When solving the dispersion equation Equation (36) numerically we take $\zeta = 100$ and $\chi = 1$. Then it follows from Equation (44) that $\beta_1 = \beta_2 = \beta$. In Figure 3 the dependence of the maximum instability increment σ_{m} on α is shown for three values of β, and in the approximation of incompressible plasma, where it is given by Equation (49). We can see that when β decreases, σ_m also decreases. In general, the effect is fairly weak. It is more pronounced for large values of α and practically negligible when $\alpha \lesssim 15^\circ$. When $\beta = 0.01$, which practically can be considered as the approximation of cold plasma, the maximum instability increment is only slightly less than that obtained in the approximation of incompressible plasma. The instability increment takes its maximum at $\kappa = \overline{\kappa}_{\mathrm{m}}$. Figure 4 shows the dependence of $\overline{\kappa}_{\mathrm{m}}/\overline{\kappa}_{\mathrm{c}}$ on α for three values of β, and in the approximation of incompressible plasma, where $\overline{\kappa}_{\mathrm{m}}/\overline{\kappa}_{\mathrm{c}} = \frac{1}{2}$ (recall that the critical dimensionless wavenumber $\overline{\kappa}_{\mathrm{c}}$ is independent of β).

Figure 5 displays the dependence on ϕ of the maximum instability increment with respect to κ. In this figure we also see that σ decreases when β decreases, and the effect is more pronounced for large values of α. The instability increment taken its maximum value at $\phi = \phi_{\mathrm{m}}$. We see that the reduction in the instability increment due to the compressibility increases with the increase of $|\phi - \phi_{\mathrm{m}}|$. When α and β are fixed the instability increment takes its maximum at $\kappa = \kappa_{\mathrm{m}}(\phi)$.

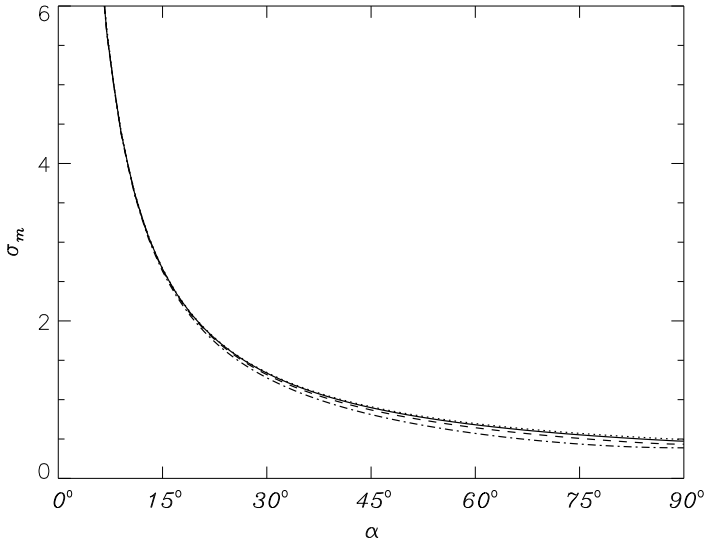

Figure 3. Dependence of the maximum instability increment $\sigma_{\rm m} = \max_{\kappa,\phi} \sigma$ on α. The solid, dashed, and dashed-dotted curves correspond to $\beta = 5$, 1, and 0.01, respectively, while the dotted line corresponds to the approximation of incompressible plasma, where the instability decrement is defined by Equation (49).

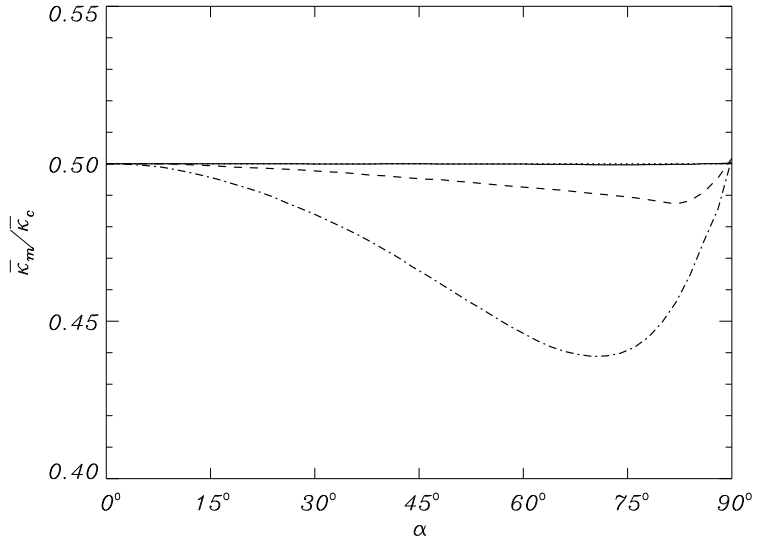

Figure 4. Dependence of $\overline{\kappa}_{\rm m}/\overline{\kappa}_{\rm c}$ on α. The solid, dashed, and dashed-dotted curves correspond to $\beta = 5$, 1, and 0.01, respectively, while the dotted line corresponds to the approximation of incompressible plasma, where $\overline{\kappa}_{\rm m}/\overline{\kappa}_{\rm c} = \frac{1}{2}$. The solid and dotted lines are practically indistinguishable.

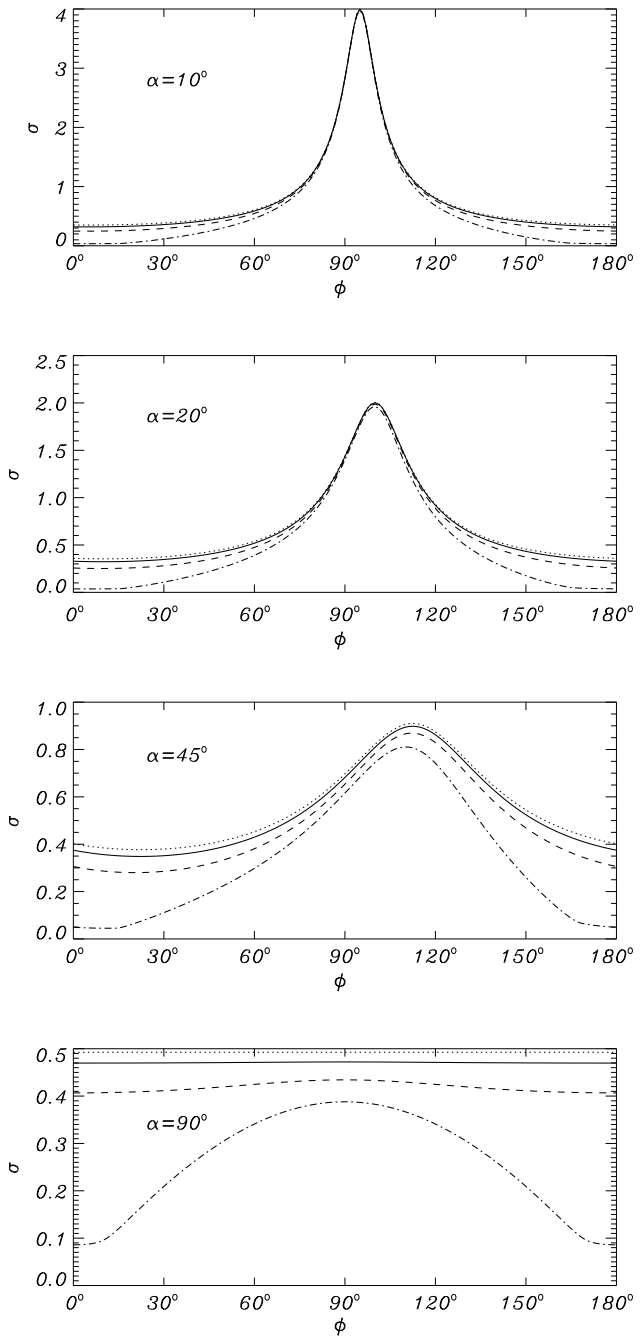

Figure 5. Dependence on ϕ of the maximum instability increment with respect to κ for four values of α: 10°, 20°, 45°, and 90°. The solid, dashed, and dashed-dotted lines correspond to $\beta = 5$, 1, and 0.01, respectively, while the dotted line corresponds to the approximation of incompressible plasma, where the instability decrement is defined by Equation (48).

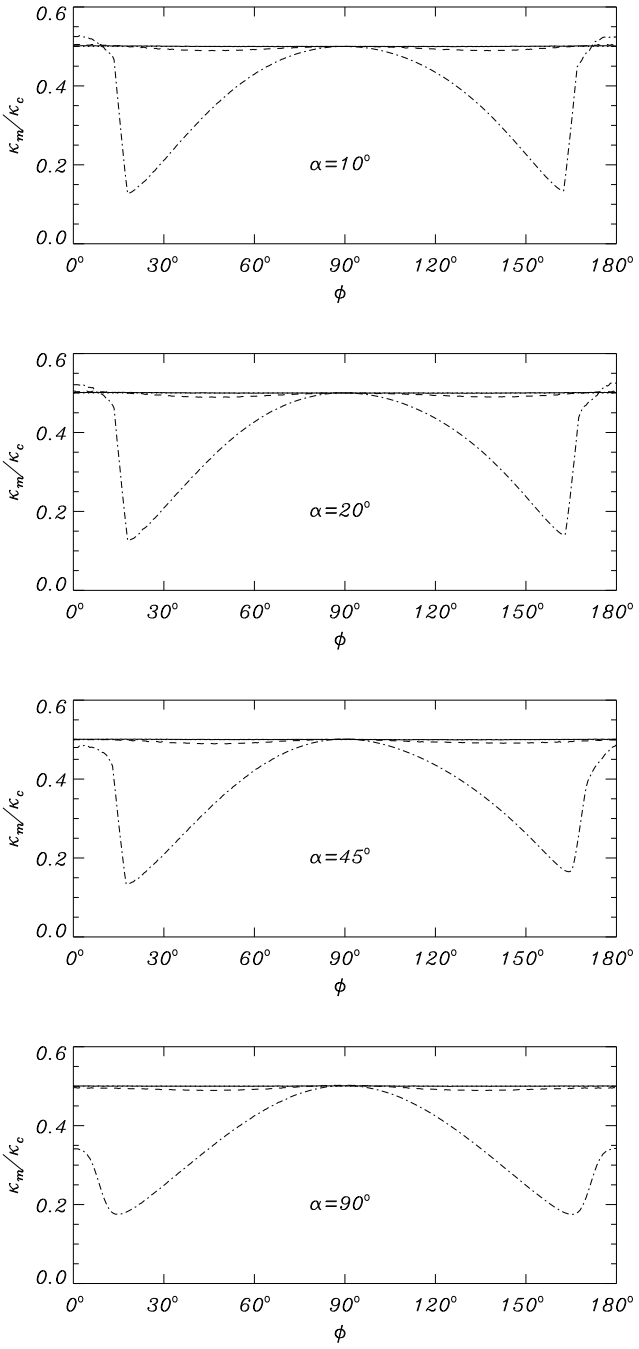

Figure 6. Dependence of $\kappa_{\rm m}/\kappa_{\rm c}$ on ϕ for four values of α: 10°, 20°, 45°, and 90°. The solid, dashed, and dashed-dotted lines correspond to $\beta = 5$, 1, and 0.01, respectively, while the dotted line corresponds to the approximation of incompressible plasma, where $\kappa_{\rm m}/\kappa_{\rm c} = \frac{1}{2}$. The solid and dotted lines are practically indistinguishable.

The dependence of $\kappa_{\rm m}$ on ϕ is shown in Figure 6 (recall that $\kappa_{\rm c}(\phi)$ is independent of β).

It is worth noting an interesting behaviour of the maximum instability increment in the case of orthogonal magnetic fields at the two sides of the interface shown in the lowest panel in Figure 5. While it depends on ϕ in a compressible plasma, it becomes independent of ϕ in the limit of incompressible plasma. Hence, the account of compressibility in the case of 90° magnetic shear destroys the isotropic nature of instability that we have in the incompressible case. In fact, there is nothing special about the equations governing the instability in the case of compressible plasma when $\alpha = 90°$. Hence, it is more correct to consider the isotropic nature of instability in the limit of incompressible plasma as a remarkable property. To understand why it occurs we briefly discuss the derivation of the dispersion equation in the case of incompressible plasma. In general, the expression for the normal velocity satisfying the continuity condition at the interface given by Equation (31) depends on ϕ. However, in the limit of incompressible plasma ($c_{\rm s} \to \infty$) it reads

$$v_z = \begin{cases} {\rm e}^{kz}, & z < 0, \\ {\rm e}^{-kz}, & z > 0, \end{cases} \tag{54}$$

which is independent of ϕ. The expression for the total pressure perturbation given by Equation (33) reduces to

$$P = \frac{i}{\omega k} \begin{cases} \rho_1\big(\omega^2 - k^2 c_{\rm A1}^2 \sin^2\phi\big){\rm e}^{kz}, & z < 0, \\ -\rho_2\big(\omega^2 - k^2 c_{\rm A2}^2 \cos^2\phi\big){\rm e}^{-kz}, & z > 0, \end{cases} \tag{55}$$

where we have substituted $\alpha = 90°$. We see that P still depends on ϕ. The instability increment is determined by the dispersion equation that is obtained by substituting Equations (54) and (55) in the boundary condition Equation (24). It reads

$$(\rho_2 + \rho_1)\omega^2 + (\rho_2 - \rho_1)gk - \rho_2 c_{\rm A2}^2 k^2(\cos^2\phi + \chi\sin^2\phi) = 0. \tag{56}$$

When the magnetic field magnitude is the same at the two sides of the interface ($\chi = 1$) this dispersion equation is independent of ϕ. We see that the instability has the isotropic nature in the approximation of incompressible plasma when $\alpha = 90°$ and $\chi = 1$ because in this case both the jumps of the normal velocity and the total pressure across the interface are independent of ϕ, *i.e.* they are isotropic.

It is expedient to compare the results presented in this section with those obtained in studies of the compressibility effect on the Rayleigh-Taylor instability in unmagnetised fluids and the MRT instability in equilibria with the unidirectional magnetic field. Both Baker (1983) and Livescu (2004) compared the RT instability increment in a compressible fluid with that in an incompressible fluid. These authors considered two equilibria in the incompressible fluid. In the first one the density varies exponentially in the same way as in the compressible fluid. In the second the density is constant above and below the interface. Since we only

considered short wavelength perturbations and neglected the density variation above and below the interface, only the second equilibrium is relevant for the present study. Both Baker (1983) and Livescu (2004) found that the instability increment in the compressible fluid is smaller than that in the incompressible fluid with the constant density. We obtaine the same result in the case of the MRT instability with the magnetic shear. Livescu (2004) also studied the effect of surface tension. It has the same effect as the magnetic shear and introduces the critical wavenumber. Perturbations with wavenumber larger than the critical one are stable.

Liberatore and Bouquet (2008) and Liberatore *et al.* (2009) studied the MRT instability. They considered equilibria with a unidirectional magnetic field, and with perturbations with wavevectors that are either parallel or perpendicular to the magnetic field. In both cases the increment in a compressible plasma is smaller than that in an incompressible plasma with constant density at both sides of the interface, which is similar to the result obtained in this paper. Perturbations propagating perpendicular to the magnetic field are unstable for any wavenumber. However perturbations propagating along the magnetic field are only unstable when the wavenumber is less than the critical one, so their behaviour is similar to that found in this paper.

Stone and Gardiner (2007a) and Stone and Gardiner (2007b) numerically studied the nonlinear evolution of the MRT instability for various forms of the equilibrium magnetic field. In particular, Stone and Gardiner (2007b) studied the instability in the equilibrium with magnetic field that is constant and has the same magnitude but different direction at the two sides of the interface. In their numerical study the authors took the ratio of the equilibrium plasma and magnetic pressure equal to 480, which corresponds to $\beta_1 = \beta_2 = 400$. Hence, at least the linear stage of the MRT instability in their model can be described in the approximation of incompressible plasma. Stone and Gardiner (2007b) found that the increment in the case where the angle between the magnetic field above and below the interface is 45° is larger than that in the case where this angle is 90°, which is in complete agreement with Equation (49). They also found that the distance between the fingers is of the order of the critical wavelength, which is in agreement with the result that the increment takes its maximum at a wavelength equal to the doubled critical wavelength.

5. MRT Instability of Prominence Threads

In this section we apply the theoretical results obtained in this article to the stability of prominence threads. Okamoto *et al.* (2007) presented the results of observations of prominence thread oscillations obtained using *Hinode*. On the basis of these results Ruderman, Terradas, and Ballester (2014) estimated that the lifetime of the thread was about 10 min. They then suggested that the thread disappearance was caused by the Rayleigh-Taylor instability and its lifetime was equal to the inverse increment of the fastest growing mode. This enabled them to estimate the magnetic shear angle α. However the assumption that the thread lifetime is equal to the inverse increment of the fastest growing

mode does not look realistic. In addition, Ruderman, Terradas, and Ballester (2014) took too large an Alfvén speed in the prominence plasma (500 $\mathrm{km\,s^{-1}}$). Hence, we reconsider their analysis.

We expect that α will be small. Then we can use Equation (53). For large ζ and $\chi = 1$ it reduces to

$$\overline{\kappa}_{\mathrm{m}} \approx \frac{1}{\alpha^2}, \quad \sigma_{\mathrm{m}} = \frac{1}{\alpha\sqrt{2}}, \tag{57}$$

where α is measured in radians. The MRT instability can only destroy a prominence thread when it reaches the nonlinear stage. In this stage fingers of heavy plasma grow in the light plasma. This nonlinear growth is fairly fast. Stone and Gardiner (2007a) showed that their length is proportional to t^2. It seems to be reasonable to assume that the thread disappearance time is a few times larger than the MRT instability growth time. We assume that the ratio of these two times is between 3 and 5, and take $g \approx 274$ $\mathrm{m/s^2}$ and $c_{\mathrm{A}2} = 100$ km/s as the typical values of the gravity acceleration and Alfvén velocity in the dense prominence plasma. Then, using Equation (57), we obtain $13^\circ \lesssim \alpha \lesssim 23^\circ$.

In our analysis we assume that the equilibrium quantities are constant above and below the interface. As explained in Section 2, this assumption can only be used if the inverse perturbation wavenumber is much smaller that the characteristic scale of the equilibrium quantity variation in the vertical direction. Let us obtain the corresponding estimates. Taking the typical value of the ratio of plasma to magnetic pressure $\bar{\beta} = 0.01$ we obtain from Equation (10) $H_2 \approx 50$ Mm, so $H_2 \approx H_1$. On the other hand, using Equation (57) we obtain for the inverse wave number of the fastest growing mode, $1/k_{\mathrm{m}} = c_{\mathrm{A}2}^2 (g\bar{\kappa}_m)^{-1}$, giving the estimate 2 Mm $\lesssim 1/k_{\mathrm{m}} \lesssim 6$ Mm. Hence, $1/k_{\mathrm{m}}$ is much smaller than H_1 and H_2. However $1/k_{\mathrm{m}}$ is larger than the characteristic thickness of prominence threads, which is 1 Mm. This makes somewhat questionable the application of results obtained in this paper to the MRT instability of prominence threads.

One more condition for the applicability of analysis presented in this article is that the MRT instability growth time is much smaller than the growth time of convective instability in the plasma in region 2. The latter growth time is $c_{\mathrm{A}2}/g \approx 6$ min. Since we assume that the ratio of the prominence lifetime to the MRT instability growth time is between 3 and 5, the instability growth time is between 2 and 3.3 min, so it is substantially smaller than the growth time of the convective instability.

Ryutova *et al.* (2010) reported the results of two observations of the MRT instability in prominences. The observed instability increments were 8.06×10^{-3} $\mathrm{s^{-1}}$ and 6.07×10^{-3} $\mathrm{s^{-1}}$. They then used the expression for the MRT instability increment in the presence of unidirectional magnetic field. They arbitrarily considered perturbations with the wavevector at an angle of 85° with respect to the magnetic field, and fit the wavelengths to obtain the observed instability increments. We use the observational results reported by Ryutova *et al.* (2010) to estimate the shear angle α. We take the same values of the equilibrium quantities as Ryutova *et al.* (2010): $\rho_2 = 8.5 \times 10^{-11}$ $\mathrm{kg\,m^{-3}}$ and $B_2 = 6$ G. Then we obtain $c_{\mathrm{A}2} \approx 60$ $\mathrm{km\,s^{-1}}$. We also take $g = 274$ $\mathrm{m\,s^{-2}}$ and assume that the magnetic field magnitude is the same at both sides of the

interface, meaning that $\chi = 1$. Ryutova *et al.* (2010) took $\zeta = 50$, however the expressions for the instability increment and the wavelength at which it is obtained are practically independent of ζ when $\zeta \gg 1$. As before, we expect to obtain small values of α. This implies that $\sigma_{\rm m}$ and $\overline{\kappa}_{\rm m}$ are approximately given by Equation (57).

We obtain $\alpha \approx 23^\circ$ in the first case, and $\alpha \approx 30^\circ$ in the second case. Using Equation (57) we obtain for the inverse wave number of the fastest growing mode $1/k_{\rm m} \approx 2$ Mm in the first case, and $1/k_{\rm m} \approx 3.6$ Mm in the second case. Hence, again $1/k_{\rm m}$ is much smaller than the atmospheric scale height, but larger than the typical thickness of prominence threads. The convective instability increment in the plasma in region 2 is $g/v_{\rm A2} \approx 4.6 \times 10^{-3}$ s^{-1}. Whilst this is smaller than the MRT instability increment, the difference is not very big.

6. Summary and Conclusions

In this article we study the Rayleigh-Taylor instability of a horizontal magnetic interface in an ideal compressible plasma. We assume that there is magnetic shear, that is the equilibrium magnetic field has different direction above and below the interface. We neglect the variation of the equilibrium quantities in the vertical direction, which is the direction perpendicular to the interface. We search for solutions in the form of normal modes and derive the dispersion equation determining the instability increment.

The main consequence of the presence of magnetic shear is that only the normal modes with a wavenumber smaller than the critical one are unstable, and the instability increment is bounded. The critical wavenumber depends on the angle ϕ between the wave vector $\boldsymbol{k}$ and the equilibrium magnetic field above the interface $\boldsymbol{B}_2$. All normal modes with the wavenumber larger than the maximum of the critical wavenumber with respect to ϕ are stable.

In the approximation of incompressible plasma the dispersion equation reduces to that derived by Ruderman, Terradas, and Ballester (2014). The critical wavenumber is independent of the plasma β and equal to that obtained in the approximation of incompressible plasma.

In the general case the dispersion equation is investigated under the assumption that the magnetic field magnitude is the same above and below the interface, and the same is true for the plasma beta. We also fix the ratio of plasma densities above and below the interface and take it equal to 100. The maximum instability increment depends on β and the shear angle α. We calculate its dependence on α for various values of β. We find that the instability decrement is a monotonically decreasing function of α. It also decreases when β is reduced, this effect being more pronounced for large values of α. When $\alpha \lesssim 15^\circ$ the maximum instability increment is almost independent of β.

We also calculate the dependence on ϕ of the maximum instability increment with respect to k. Again we find that the increment decreases when β is reduced, and again the effect is more pronounced for large values of α. The instability increment takes a maximum at $\phi = \phi_{\rm m}$. The effect of reduction of the instability increment when β decreases is stronger for large values of $|\phi - \phi_{\rm m}|$.

The theoretical results obtained in this article are applied to the observations of the MRT instability in prominence threads. We use the observations of prominence thread disappearance reported by Okamoto *et al.* (2007), and the observed MRT instability increment in prominence threads given by Ryutova *et al.* (2010). We obtain fairly reasonable estimates for the shear angle α varying from 13° to 30°. In all cases the inverse of the wave number of the most unstable mode is much smaller than the atmospheric scale heights at both sides of the interface. The plasma above the interface is convectively unstable, however the MRT instability increment is larger than that of the convective instability, meaning that the effect of convective instability can be neglected. The weakest point of this analysis is that the inverse of the wave number of the most unstable mode is larger than the typical thickness of prominence threads. This implies that the next step of studying the MRT instability of prominence threads should be the extension of the analysis to an equilibrium that consists of a slab of cold dense plasma sandwiched with two semi-infinite regions with hot rarefied plasma.

Acknowledgements MSR acknowledges the support by the STFC grant.

Disclosure of Potential Conflicts of Interests The author declare that he has no conflicts of interest.

Appendix

A. Derivation of Equations (25) and (26)

In this section we derive Equations (25) and (26). Using Equations (7), (18), (22), and (23) we transform Equations (19), (20), and the expression for P to

$$\boldsymbol{v}_\perp = \frac{\boldsymbol{k}P}{\rho\omega} - \frac{c_\mathrm{A} k\cos\varphi}{\omega\sqrt{\mu_0\rho}}\boldsymbol{b}_\perp, \tag{58}$$

$$iv_z = \frac{1}{\rho\omega}\frac{\mathrm{d}P}{\mathrm{d}z} + \frac{ic_\mathrm{A}^2 k^2\cos^2\varphi}{\omega^2}v_z + \frac{g}{\omega^2}\left(\boldsymbol{k}\cdot\boldsymbol{v}_\perp - i\frac{\mathrm{d}v_z}{\mathrm{d}z}\right), \tag{59}$$

$$P = \frac{\rho c_\mathrm{s}^2}{\omega}\left(\boldsymbol{k}\cdot\boldsymbol{v}_\perp - i\frac{\mathrm{d}v_z}{\mathrm{d}z}\right) + \frac{\boldsymbol{B}\cdot\boldsymbol{b}_\perp}{\mu_0}. \tag{60}$$

Now we use Equation (21) to eliminate $\boldsymbol{b}_\perp$ from Equations (58) and (60). As a result we obtain

$$\Omega_\mathrm{A}\boldsymbol{v}_\perp = \frac{\omega\boldsymbol{k}P}{\rho} - \frac{c_\mathrm{A} k\boldsymbol{B}\cos\varphi}{\sqrt{\mu_0\rho}}\left(\boldsymbol{k}\cdot\boldsymbol{v}_\perp - i\frac{\mathrm{d}v_z}{\mathrm{d}z}\right), \tag{61}$$

$$P = \frac{\rho(c_\mathrm{s}^2 + c_\mathrm{A}^2)}{\omega}\left(\boldsymbol{k}\cdot\boldsymbol{v}_\perp - i\frac{\mathrm{d}v_z}{\mathrm{d}z}\right) - \frac{\rho c_\mathrm{A}^2 k\cos\varphi}{\omega B}\boldsymbol{B}\cdot\boldsymbol{v}_\perp. \tag{62}$$

Taking the scalar product of Equation (61) with $\boldsymbol{k}$ and $\boldsymbol{B}$ yields

$$\boldsymbol{k}\cdot\boldsymbol{v}_\perp = \frac{k^2 P}{\rho\omega} + \frac{ic_{\rm A}^2 k^2\cos^2\varphi}{\omega^2}\frac{{\rm d}v_z}{{\rm d}z}, \tag{63}$$

$$\boldsymbol{B}\cdot\boldsymbol{v}_\perp = \frac{kB\cos\varphi}{\Omega_{\rm A}}\left(\frac{\omega}{\rho}P + ic_{\rm A}^2\frac{{\rm d}v_z}{{\rm d}z} - c_{\rm A}^2\boldsymbol{k}\cdot\boldsymbol{v}_\perp\right). \tag{64}$$

Using Equations (63) and (64) to eliminate $\boldsymbol{v}_\perp$ from Equations (59) and (62) we eventually arrive at Equations (25) and (26).

References

Baker, L.: 1983, *Phys. Fluids* **26**, 950. doi:10.1063/1.864245.

Bucciantini, N., Amato, E., Bandiera, R., Blondin, J.M., Del Zanna, L.: 2004, *Astron. Astrophys.* **423**, 253. doi:10.1051/0004-6361:20040360.

Díaz, A.J., Khomenko, E., Collados, M.: 2014, *Astron. Astrophys.* **564**, A97. doi:10.1051/0004-6361/201322147.

Goedbloed, J.P.H., Poedts, S.: 2004, *Principles of Magnetohydrodynamics*, Cambridge University Press, Cambridge, UK.

Hillier, A., Isobe, H., Shibata, K., Berger, T.: 2011, *Astrophys. J. Lett.* **736**, L1. doi:10.1088/2041-8205/736/1/L1.

Hillier, A., Berger, T., Isobe, H., Shibata, K.: 2012a, *Astrophys. J.* **746**, 120. doi:10.1088/0004-637X/746/2/120.

Hillier, A., Isobe, H., Shibata, K., Berger, T.: 2012b, *Astrophys. J.* **756**, 110. doi:10.1088/0004-637X/756/2/110.

Isobe, H., Miyagoshi, T., Shibata, K., Yokoyama, T.: 2005, *Nature* **434**, 478. doi:10.1038/nature03399.

Isobe, H., Miyagoshi, T., Shibata, K., Yokoyama, T.: 2006, *PASJ* **58**, 423. doi:10.1093/pasj/58.2.423.

Jones, T.W., De Young, D.S.: 2005 *Astrophys. J.* **624**, 586. doi:10.1086/429157.

Jun, B.I., Norman, M.L.: 1996, *Astrophys. J.* **472**, 245. doi:10.1086/178059.

Jun, B.I., Norman, M.L., Stone, J.M.: 1995, *Astrophys. J.* **453**, 332. doi:10.1086/176393.

Khomenko, E., Díaz, A.J., de Vicente, A., Collados, M., Luna, M.: 2014, *Astron. Astrophys.* **565**, A45. doi:10.1051/0004-6361/201322918.

Liberatore, S., Bouquet, S.: 2008, *Phys. Fluids* **20**, 116101. doi:10.1063/1.3025832.

Liberatore, S., Jaouen, S., Tabakhoff, E., Canaud B.: 2009, *Phys. Plasmas* **16**, 044502. doi:10.1063/1.3109664.

Livescu, D.: 2004, *Phys. Fluids* **16**, 118. doi:10.1063/1.1630800.

Newcomb, W.A.:1961, *Phys. Fluids* **4**, 391. doi:10.1063/1.1706342.

Okamoto, T.J., Tsuneta, S, Berger, T.E., Ichimoto, K., Katsukawa, Y., Lites, B.W., *et al.*: 2007, *Science* **318**, 1577. doi:10.1126/science.1145447.

Owen, S.M., De Young, D.S., Jones, T.W.: 2009, *Astrophys. J.* **694**, 1317. doi:10.1088/0004-637X/694/2/1317.

Robinson, D., Dursi, L.J., Ricker, P.M., Rosner, R., Calder, A.C., Zingale, M., *et al.*: 2004, *Astrophys. J.* **601**, 621. doi:10.1086/380817.

Ruderman, M.S.: 2015, *Astron. Astrophys.* **580**, A37. doi:10.1051/0004-6361/201525959

Ruderman, M.S., Terradas, J., Ballester, J.L.: 2014, *Astrophys. J.* **785**, A110. doi:10.1051/0004-6361/201016172

Ryutova, M.P., Berger, T., Frank, Z., Tarbell, T., Title, A.: 2010, *Sol. Phys.* **267**, 75. doi:10.1007/s11207-010-9638-9.

Stone, J.M., Gardiner, T.: 2007a *Phys. Fluids* **19**, 094104. doi:10.1063/1.2767666.

Stone, J.M., Gardiner, T.: 2007b *Astrophys. J.* **671**, 1726. doi:10.1086/523099.

Terradas, J., Oliver, R., Ballester, J.L.: 2012, *Astron. Astrophys.* **541**, A102. doi:10.1051/0004-6361/201219027

Yu, C.P.: 1965, *Phys. Fluids* **8**, 650. doi:10.1063/1.1761278